

EXCESS GALACTIC MOLECULAR ABSORPTION TOWARD THE RADIO GALAXY 3C 111

F. TOMBESI^{1,2,3}, C. S. REYNOLDS², R. F. MUSHOTZKY² AND E. BEHAR⁴

¹X-ray Astrophysics Laboratory, NASA/Goddard Space Flight Center, Greenbelt, MD 20771, USA; francesco.tombesi@nasa.gov

²Department of Astronomy, University of Maryland, College Park, MD 20742, USA; ftombesi@astro.umd.edu

³Department of Physics, University of Rome “Tor Vergata”, Via della Ricerca Scientifica 1, I-00133 Rome, Italy;

francesco.tombesi@roma2.infn.it

and

⁴Department of Physics, Technion 32000, Haifa 32000, Israel

ABSTRACT

We show the combined spectral analysis of *Chandra* high energy transmission grating (HETG) and *XMM-Newton* reflection grating spectrometer (RGS) observations of the broad-line radio galaxy 3C 111. The source is known to show excess neutral absorption with respect to the one estimated from 21 cm radio surveys of atomic H I in the Galaxy. However, previous works were not able to constrain the origin of such absorber as local to our Milky Way or intrinsic to the source ($z = 0.0485$). The high signal-to-noise grating spectra allow us to constrain the excess absorption as due to intervening gas in the Milky Way, and we estimate a time averaged total column density of $N_H = (7.4 \pm 0.1) \times 10^{21} \text{ cm}^{-2}$, a factor of two higher than the tabulated H I value. We recommend to use the total average Galactic column density here estimated when studying 3C 111. The origin of the extra Galactic absorption of $N_H = 4.4 \times 10^{21} \text{ cm}^{-2}$ is likely due to molecular gas associated with the Taurus molecular cloud complex toward 3C 111, which is our nearest star-forming region. We also detect a weak ($\text{EW} = 16 \pm 10 \text{ eV}$) and narrow ($\text{FWHM} < 5,500 \text{ km s}^{-1}$, consistent with optical H α) Fe K α emission line at $E = 6.4 \text{ keV}$ likely from the torus in the central regions of 3C 111, and we place an upper limit on the column density of a possible intrinsic warm absorber of $N_H < 2.5 \times 10^{20} \text{ cm}^{-2}$. These complexities make 3C 111 a very promising object for studying both the intrinsic properties of this active radio galaxy and the Galactic interstellar medium if used as a background source.

Keywords: Galaxy: local interstellar matter — galaxies: active — X-rays: galaxies — X-rays: ISM

1. INTRODUCTION

Active galactic nuclei (AGN) are classified in two main categories as radio-loud and radio-quiet AGN, depending on their radio luminosity with respect to optical (Kellerman et al. 1989). The origin of this dichotomy is still not known, but it is manifested by the presence of powerful, often relativistic, radio jets in radio-loud AGN (e.g., Urry & Padovani 1995). On the other hand, radio-quiet AGN, most notably Seyfert galaxies and quasars, show clear features of massive, sub-relativistic winds (e.g., Tombesi et al. 2010a; Gofford et al. 2015). Although, winds have been recently reported in radio-loud sources as well (e.g., Reeves et al. 2009; Torresi et al. 2010, 2012; Tombesi et al. 2010b, 2014; Gofford et al. 2015).

The X-ray band is particularly promising for inves-

tigating the possible origin of such dichotomy because the radiation is emitted close to the central supermassive black hole (SMBH), and therefore it can retain information from both the accretion disk and intervening absorption and emission in the regions surrounding the AGN or the host galaxy interstellar medium (e.g. Sambruna et al. 1999, 2011; Ogle et al. 2005; Lewis et al. 2005; Ballo et al. 2011; Braito et al. 2011; Tombesi et al. 2011, 2016; Lohfink et al. 2015). Coordinated observations in the X-ray, optical, and radio allowed also to study the connection between the disk, jet and winds in some sources (e.g., Chatterjee et al. 2011; Tombesi et al. 2012; Lohfink et al. 2013).

Here, we report on the analysis of a long 150 ks *Chandra* HETG observation of the broad-line radio galaxy (BLRG) 3C 111 ($z = 0.0485$), in combination with

archived *XMM-Newton* RGS spectra. This is the third paper of this series, the previous two focused on 3C 390.3 and 3C 120, respectively (Tombesi et al. 2016, 2017). The radio galaxy 3C 111 is an X-ray bright BLRG and it is classified as a Fanaroff–Riley type II (FRII) source with a double-lobe/single-jet morphology (Linfield & Perley 1984). The inner jet has been seen to display superluminal motion (Vermeulen & Cohen 1994; Chatterjee et al. 2011). This source was also detected in the γ -ray band with Fermi (Kataoka et al. 2011; Grandi et al. 2012).

The main objective of the *Chandra* HETG campaign was to study the possible X-ray warm absorbers in the brightest radio galaxies. However, we do not find significant evidence for an intrinsic soft X-ray ionized absorber in this source. The apparent lack of a warm absorber is puzzling due to the fact that 3C 111 shows powerful jets and accretion disk winds driven by the central supermassive black hole (e.g., Tombesi et al. 2010b; Chatterjee et al. 2011). Moreover, warm absorbers have been detected in most bright radio galaxies (e.g., Reeves et al. 2009; Torresi et al. 2010, 2012; Braito et al. 2011). On the other hand, this source is known to show an excess of cold/neutral absorption with respect to the value estimated from 21 cm radio surveys of atomic H I. Previous X-ray studies have not been able to constrain the origin of such absorber as local to our Milky Way or intrinsic to 3C 111 because the redshift could not be constrained (e.g., Reynolds et al. 1998; Lewis et al. 2005; Ballo et al. 2011; Tombesi et al. 2013).

We note that 3C 111, along with other bright AGN, has been used as an extragalactic background radio source to explore complex atomic and molecular gas regions in the Milky Way (e.g., Marscher, Moore & Bania 1993; Moore & Marscher 1995). In fact, 3C 111 is located at a relatively low latitude with respect to the Galactic plane and it lies behind the giant Taurus molecular cloud, which is the nearest large star-forming region in our Galaxy (Ungerer et al. 1985; Ungerechts & Thaddeus 1987).

Several detailed studies of the structure in the atomic component of the interstellar medium (ISM) have suggested that complexities exist on scales as small as few tens of AU. The first indication that such small-scale H I structures may exist was reported by Dieter, Welch, & Romney (1976). Using VLBI techniques to measure changes in the visibility function in the Galactic H I absorption line toward 3C 147, they proposed that the line variations were due to a small cloud with dimension of about 70 AU and a density of $\simeq 10^5$ atoms cm^{-3} .

Moreover, Faison et al. (1998) used VLBA and the VLA to image Galactic H I in absorption in the direction of three other bright extragalactic sources, namely 3C 138, 2255+416, and CJ1 0404+768. They sug-

gested that the small-scale opacity structures seen toward 3C 138 and 2255+416 may be due to density variations, spin temperature variations, velocity turbulence in the atomic gas, or a combination of these effects. If the opacity variations are due to fluctuations in density, then they would suggest clouds with high densities of $\sim 10^6$ cm^{-3} in the cold neutral medium on ~ 10 AU scales.

Besides atomic H I, there has been evidence for small-scale structures also in the diffuse molecular gas in our Galaxy. For instance, Moore & Marscher (1995) reported changes in the column density of formaldehyde (H_2CO) toward the compact sources NRAO 150, 3C 111, and BL Lac. They observed the three sources for over 3 yrs with the VLA in the 6 cm H_2CO line. The motion of the sources due to parallax as well as the proper motions of the absorbing gas caused the relative line of sight through the molecular gas to the extragalactic sources to change with time. They observed significant variations in the molecular column density toward NRAO 150 and 3C 111, which indicate structures on the scales of ~ 10 AU and densities of $\sim 10^6$ cm^{-3} . Several other studies have been performed in order to map the molecular OH and CO distribution in the Galaxy using compact background continuum sources in the radio and mm-waves (e.g., Liszt & Lucas 1996, 1998).

In the X-ray band, compact X-ray binaries have provided important information regarding the composition and ionization of the Galactic ISM through absorption, although such sources are mostly distributed along the galactic plane (e.g., Schulz et al. 2002; Gatuzz et al. 2015). Some attempts to use bright extragalactic continuum sources to explore our Galaxy multi-phase and multi-scale ISM along several lines of sight have also been reported in the UV and X-ray bands, for instance recently in the context of the origin of the *Fermi* bubbles (e.g., Fox et al. 2015; Nicastro et al. 2016; Bordoloi et al. 2017).

A complementary method to explore the atomic and molecular hydrogen content from many different sightlines in the Milky Way is provided by gamma-ray bursts (GRBs) afterglows in the X-ray band. We note that the value reported for the cold absorption toward 3C 111 is about a factor of two higher than the upper limit reported by Willingdale et al. (2013) for GRB sightlines.

2. DATA ANALYSIS AND RESULTS

We describe the analysis of the *Chandra* HETG spectrum of the broad-line radio galaxy 3C 111. It was observed on November 4th 2014 for a single exposure of 143 ks (ID 16219). The spectrum was extracted using the *CIAO* package v4.7. Only the first order dispersed spectra were considered for both the Medium Energy Grating (MEG) and High Energy Grating (HEG), and

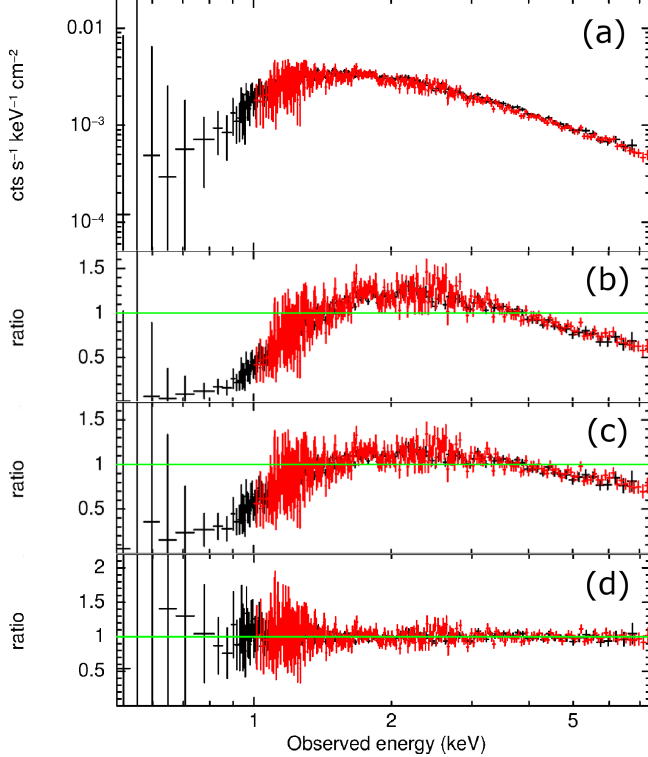


Figure 1. *Chandra* MEG (black) and HEG (red) spectra of 3C 111. The data are binned to $4 \times$ the FWHM resolution and to a minimum signal-to-noise of 2 in order to emphasize the broad-band curvature of the spectrum due to the absorber column density. *Panel a:* MEG and HEG spectra. *Panel b:* ratio with respect to a power-law continuum model. *Panel c:* ratio with respect to a power-law continuum model including the tabulated Galactic absorption value of $N_H = 3 \times 10^{21} \text{ cm}^{-2}$. *Panel d:* ratio with respect to the best-fit model consisting of a power-law continuum, Galactic absorption with free column density and an Fe K α emission line.

the ± 1 orders for each grating were subsequently combined for each sequence. The background count rate is found to be negligible. The resultant spectra were binned to the full width half maximum (FWHM) of their spectral resolution, which corresponds to $\Delta\lambda = 0.023 \text{ \AA}$ and $\Delta\lambda = 0.012 \text{ \AA}$ bins for MEG and HEG, respectively. The MEG and HEG spectra were analyzed in the energy bands $E=0.5\text{--}7 \text{ keV}$ and $E=1\text{--}7.5 \text{ keV}$, respectively. The MEG and HEG count rates are 0.47 cts s^{-1} and 0.28 cts s^{-1} , respectively. The spectral analysis was performed using the software *XSPEC* v.12.8.2 and the C-statistic was applied. We performed simultaneous fits of the MEG and HEG spectra considering a free cross-normalization constant, which resulted being always very close to unity. All parameters are given in the source rest frame and the errors and limits are at the 90% level if not otherwise stated. Standard Solar abundances are assumed (Asplund et al. 2009).

The MEG and HEG spectra of 3C 111 are shown in panel a of Fig. 1. We started the spectral modeling

using a power-law continuum with photon index $\Gamma \simeq 0.9$. As we can see from panel b of Fig. 1 this does not provide a good fit ($C/u = 8182/2220$), with the soft X-ray residuals and very flat spectral index indicating the requirement for a neutral absorption component.

We then included a neutral absorption component modeled with *tbabs* in *XSPEC*. This model calculates the cross section for X-ray absorption by the interstellar medium as the sum of the cross sections for X-ray absorption due to the gas-phase, the grain-phase, and the molecules (Wilms et al. 2000).

We start using a column density of $N_H = 3 \times 10^{21} \text{ cm}^{-2}$ derived from NASA's HEASARC *nh* tool¹. This is the intermediate value between the weighted average values estimated by the Leiden/Argentine/Bonn Survey of Galactic H I (Kalberla et al. 2005) of $N_H = 2.91 \times 10^{21} \text{ cm}^{-1}$ and by the Dickey & Lockman H I in the Galaxy (Dickey & Lockman 1990) of $N_H = 3.15 \times 10^{21} \text{ cm}^{-2}$. This fit provides a high statistical improvement with $C/u = 4145/2220$ and less flat power-law photon index of $\Gamma \simeq 1.2$. The ratio of the spectra with respect to the power-law including the tabulated Galactic absorption is shown in panel c of Fig. 1. We note an improvement with respect to panel b, but the fit is still not satisfactory.

Previous observations of the radio galaxy 3C 111 showed an excess absorption with respect to the tabulated Galactic value of $N_H \sim 5 \times 10^{21} \text{ cm}^{-2}$. However, it was still not possible to constrain the origin of such absorber as local to our Milky Way or intrinsic to 3C 111 because the redshift could not be constrained (e.g., Reynolds et al. 1998; Lewis et al. 2005; Ballo et al. 2011; Tombesi et al. 2013).

We then included a new *ztbabs* absorption component assuming the redshift of the source. We obtained a high fit improvement with $C/u = 2264/2219$ for a column density of $N_H = (5.1 \pm 0.3) \times 10^{21} \text{ cm}^{-2}$ and a photon index of $\Gamma \simeq 1.6$. We then left the redshift free to vary and we obtained an additional very high fit improvement of $\Delta C/\Delta u = 25/1$, corresponding to a statistical confidence level of 5σ . The best-fit redshift is $z = -0.002^{+0.002}_{-0.038}$, which is consistent with being local to our Milky Way galaxy instead of 3C 111 at a redshift of $z = 0.0485$. Considering a single neutral *ztbabs* absorber component to model both the tabulated and excess absorption we obtain a column density of $N_H = (7.5 \pm 0.2) \times 10^{21} \text{ cm}^{-2}$ and a better constrained redshift value of $z = -0.002^{+0.002}_{-0.008}$. The contour plots of these parameters are shown subsequently in Fig. 4.

The main spectral features responsible for the ab-

¹ <http://heasarc.gsfc.nasa.gov/cgi-bin/Tools/w3nh/w3nh.pl>

sorption are the photoelectric edges from O I K at $E=0.543$ keV, Fe I L₁ at $E=0.845$ keV, Fe I L₂ at $E=0.72$ keV, and Ne I K at $E=0.87$ keV. In particular, being the O edge so deep, the fit is mostly driven by counts in the latter three edges. In fact, we obtain the same results restricting the fit to energies higher than $E=0.7$ keV. Moreover, we note that the Fe I L₁ edge is significantly weaker than the Fe I L₂ edge, and therefore it will only marginally affect the fit (e.g., Schulz et al. 2002). We checked that we obtain the same results using different absorption models in XSPEC, such as *phabs* and *wabs*, or the detailed X-ray absorption code *tbnew_gas* (Wilms et al. 2000), which is however still at a beta-test version².

Looking at the ratio between the data and this model zoomed in the $E=6-7$ keV band in Fig. 2 we observe the presence of a faint emission line at the expected energy of the Fe K α fluorescence emission line of $E=6.4$ keV. Therefore, we consider the final best-fit model composed of a power-law continuum, a single Galactic neutral absorber, and an Fe K α Gaussian emission line. The ratio of the data with respect to the best-fit model is shown in panel d of Fig. 1.

Assuming a redshift of zero, i.e. local to our Milky Way, the best-fit parameters are a column density of $N_H = (7.7 \pm 0.1) \times 10^{21}$ cm $^{-2}$, a power-law photon index of $\Gamma = 1.62 \pm 0.02$, and an emission line at the energy of $E=6.41 \pm 0.03$ keV with intensity $I = (1.2 \pm 0.7) \times 10^{-5}$ ph s $^{-1}$ cm $^{-2}$, width $\sigma < 50$ eV, and equivalent width $EW=16 \pm 10$ eV. The best-fit statistics is $C/u = 2232/2216$. The extrapolated absorption corrected fluxes in the energy intervals $E=0.5-2$ keV and $E=2-10$ keV are 3.0×10^{-11} erg s $^{-1}$ cm $^{-2}$ and 6.1×10^{-11} erg s $^{-1}$ cm $^{-2}$, respectively.

The intensity of the Fe K α emission line is consistent with previous estimates and the low EW is consistent with the source being observed during a high state (Reynolds et al. 1998; Tombesi et al. 2010b, 2011, 2012b, 2014; Chatterjee et al. 2011; Ballo et al. 2011). We note that the full width at half maximum (FWHM) of the Fe K α of $FWMH_{FeK} < 5,500$ km s $^{-1}$ is consistent with the FWHM of the optical H α line of $FWMH_{H\alpha} = 4,800 \pm 200$ km s $^{-1}$ (Eracleous & Halpern 2003). The full width at zero intensity (FWZI) from the H α line is instead much broader $FWZI = 18,400 \pm 3,000$ km s $^{-1}$, but we can not constrain this larger broadening if present also in the Fe K α line due to the limited signal-to-noise in the spectrum at these energies.

Using an *XSTAR* photo-ionized absorption table with turbulent velocity of 100 km s $^{-1}$ and assuming the typ-

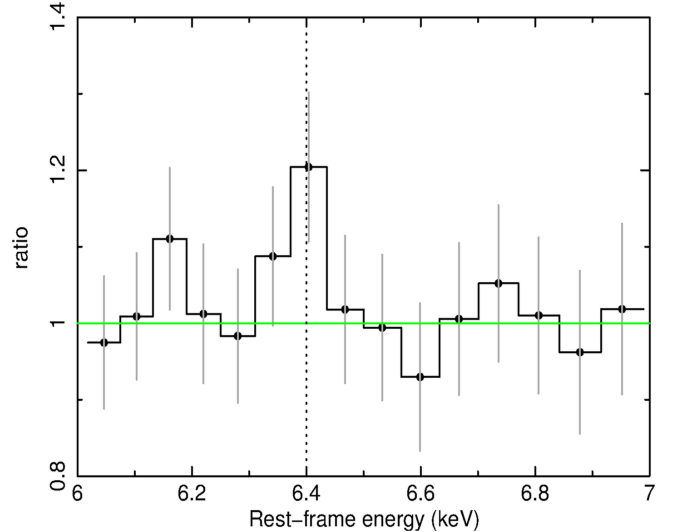


Figure 2. Ratio between the *Chandra* HEG spectrum and an absorbed power-law model zoomed in the energy band $E=6-7$ keV. The vertical dotted line indicates the Fe K α line at the energy of $E=6.4$ keV. The data are binned to $2 \times$ the FWHM resolution for clarity.

ical ionization of the warm absorber detected in other BLRGs of $\log \xi \simeq 2.5$ erg s $^{-1}$ cm and a velocity consistent with zero at the source rest-frame (e.g., Reeves et al. 2009; Torresi et al. 2010, 2012), we estimate an upper limit of the column density of a possible warm absorber of $N_H < 2.5 \times 10^{20}$ cm $^{-2}$. The fact that we do not clearly detect a warm absorber in this source could partially be due to the intervening absorption from our own Galaxy and/or to the fact that the interstellar medium in this source could be hot, as observed in 3C 390.3 and 3C 120, and the low inclination estimated at $\simeq 18^\circ$ from the radio jet (e.g., Torresi et al. 2012; Tombesi et al. 2016, 2017).

2.1. Combining *Chandra* and *XMM-Newton* spectra

3C 111 was observed twice with *XMM-Newton*, in 2001 for 45 ks and in 2009 for 120 ks. Here, our focus is on the high-energy resolution RGS spectra in the energy band between $E=0.5-2.5$ keV. We use both RGS1 and RGS2 detectors, and the latest pipeline data products.

First, we analyzed the RGS data alone using a model composed of a Galactic absorbed power-law continuum with extra cold absorption. Given the limited energy band of the RGS, we consider a power-law continuum of $\Gamma = 1.6$ as estimated from previous broadband spectral analyses of these observations (Lewis et al. 2005; Ballo et al. 2011). Also in this case we find an extra absorption column density of $N_H \simeq 5 \times 10^{21}$ cm $^{-2}$, with a redshift consistent with zero with an uncertainty of $\Delta z \simeq 0.02$. Therefore, also the RGS data alone favor an absorber in the Milky Way, with a confidence level of $\sim 4\sigma$.

We then performed a combined fit of the *Chandra* HETG and *XMM-Newton* RGS spectra allowing for free

² <http://pulsar.sternwarte.uni-erlangen.de/wilms/research/tbabs/>

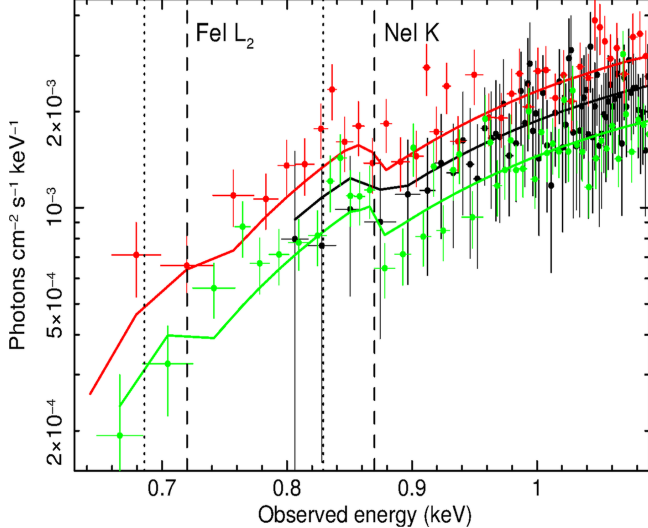


Figure 3. Grating spectra and best-fit absorbed power-law model zoomed in the $E=0.6\text{--}1.1$ keV band. The *Chandra* MEG (black) is binned to $2\times$ the FWHM resolution and to a minimum signal-to-noise of 2 for clarity. The *XMM-Newton* RGS2 spectra taken in 2001 (red) and 2009 (green) are binned to a minimum signal-to-noise of 5 for clarity. The MEG data below $E=0.8$ keV are not shown here because the large error bars would make the comparison with the RGS less clear. The vertical dashed and dotted lines indicate the edge energies for Fe I L₂ at $E=0.72$ keV and Ne I K at $E=0.87$ keV for a redshift of zero and intrinsic to 3C 111, respectively.

power-law normalizations and cross-normalizations between observations and instruments, respectively. When fitting with a redshift fixed to the one of 3C 111 ($z = 0.0485$) or free to vary for the excess absorber, we find that a value consistent with zero is favored at $> 6\sigma$ ($\Delta C/\Delta u = 43/1$).

Considering only one absorber, we estimate a power-law photon index of $\Gamma = 1.60 \pm 0.01$, a total Galactic absorption column density of $N_H = (7.4 \pm 0.1) \times 10^{21} \text{ cm}^{-2}$, and a redshift of $z = -0.002^{+0.003}_{-0.002}$. We consider this total time-averaged column density estimate to be the best-fit value from our analysis. The grating spectra and the best-fit absorbed power-law model zoomed in the $E=0.6\text{--}1.1$ keV band for the *Chandra* MEG and the *XMM-Newton* RGS2 taken in 2001 and 2009 are shown in Fig. 3. Instead, the contour plots of the column density with respect to the absorber redshift for the fits using the *Chandra* HETG and *XMM-Newton* RGS spectra alone, and both combined, are shown in Fig. 4.

Given that the three observations were performed over a time-scale of about a decade, we also performed a multi epoch spectral fit leaving the column density and redshift free to vary. We obtain that the redshift is always consistent with zero, but the column density shows a possible increase from $N_H = (7.0 \pm 0.02) \times 10^{21} \text{ cm}^{-2}$ for the *XMM-Newton* observation in 2001 to a value of $N_H = (7.5 \pm 0.02) \times 10^{21} \text{ cm}^{-2}$ for the *XMM-Newton*

and *Chandra* observations of 2009 and 2014, respectively. Although very marginal, this increase in column density is in line with the reported temporal variability in the strength and profile of the 4.83 GHz H₂CO absorption line in radio observations, which show that the cloud complex may contain inhomogeneities even on sub-parsec scales (e.g., Marscher, Moore & Bania 1993; Moore & Marscher 1995).

We checked also for variable O, Ne, and Fe abundances using the *tbvarabs* model in XSPEC (Wilms et al. 2000). The abundances are consistent with the Solar values within the uncertainties and we are able to place only lower limits of $A_{\text{O}} \geq 0.5$, $A_{\text{Ne}} \geq 0.9$, and $A_{\text{Fe}} \geq 0.9$, respectively.

Finally, we performed a consistency check analyzing also the *XMM-Newton* EPIC-pn spectra simultaneous with the RGS observations performed in 2001 and 2009. The EPIC-pn has the highest sensitivity in the energy interval $E=0.5\text{--}10$ keV. However, we note that the resolving power of the EPIC-pn of $E/\Delta E \simeq 5\text{--}10$ at the energies of $E=0.5\text{--}1.0$ keV is very limited compared to $E/\Delta E \simeq 300$ for the RGS and $E/\Delta E \simeq 600$ for the HETG, respectively. Moreover, there are significant cross-calibration uncertainties of both the shape and normalization of the effective area between the EPIC-pn and RGS.

We extracted the source and background spectra from 40 arcsec circular regions on the detectors and applied standard reduction techniques. We consider the absorbed power-law continuum model in the whole energy interval of $E=0.5\text{--}10$ keV. The column densities are estimated to be $N_H = (0.61 \pm 0.04) \times 10^{21} \text{ cm}^{-2}$ and $N_H = (0.73 \pm 0.03) \times 10^{21} \text{ cm}^{-2}$, respectively. We can place an upper limit on the redshift of the absorber of $z < 0.025$, which is lower than the one of 3C 111 of $z = 0.0485$. These values are in agreement with the much more accurate results derived from the analysis of the RGS and HETG spectra.

3. DISCUSSION

The radio galaxy 3C 111 was known from previous observations to show excess neutral absorption with respect to the column density of $N_H = 3 \times 10^{21} \text{ cm}^{-2}$ estimated from 21 cm radio surveys of H I in the Galaxy (Dickey & Lockman 1990; Kalberla et al. 2005). However, it was still not possible to constrain the origin of such absorber as local to our Milky Way or intrinsic to 3C 111 ($z = 0.0485$) because the redshift of this component could not be constrained (e.g., Reynolds et al. 1998; Lewis et al. 2005; Tombesi et al. 2013; Ballo et al. 2011). The analysis of the *Chandra* HETG and *XMM-Newton* RGS spectra of 3C 111 allowed us to constrain the excess absorption as due to intervening gas in the Milky Way and to estimate a total time-averaged

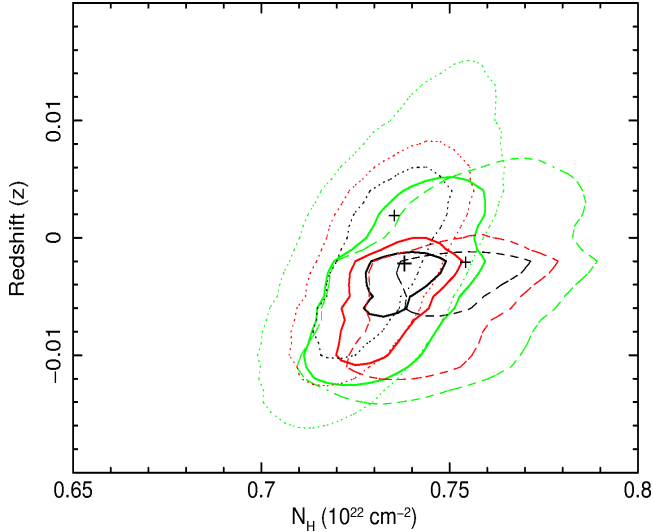


Figure 4. Contour plots comparing the column density with respect to the cosmological redshift of a single neutral absorber component modeling both the tabulated and the excess Galactic absorption. The contours refer to *Chandra* HETG (dashed), *XMM-Newton* RGS (dotted), and their combined fit (solid). The crosses indicate the best-fit values. The contours refer to confidence levels of 68% (black), 90% (red), and 99% (green), respectively.

column density of $N_H = (7.4 \pm 0.1) \times 10^{21} \text{ cm}^{-2}$. What is the origin of the extra Galactic neutral absorption of $N_H = 4.4 \times 10^{21} \text{ cm}^{-2}$ with respect to the atomic H I value?

3C 111 is located at a relatively low latitude ($b = -8.8^\circ$) with respect to the Galactic plane and it is known to lie behind the giant Taurus molecular cloud, which is the nearest large star-forming region in our Galaxy, at an estimated distance of about 200 pc from us (Ungerer et al. 1985; Ungerechts & Thaddeus 1987). Reynolds et al. (1998) suggested that this cloud complex may cause variations between the actual Galactic absorption along our line of sight and that inferred from 21 cm radio measurements due to inhomogeneities or the presence of molecular hydrogen.

Temporal variability in the strength and profile of the 4.83 GHz H₂CO absorption line in radio observations show that the cloud complex contains inhomogeneities on sub-parsec scales, and that between 30 and 100 clumps may lie along the line of sight to 3C 111 (Marscher, Moore & Bania 1993; Moore & Marscher 1995). A column density change is also marginally evident comparing the X-ray spectra performed a decade apart in sec. 2.1. These inhomogeneities could in principle partially explain the discrepancy in column density estimates, but 3C 111 does not appear to be blocked by one or more particularly dense clumps (Reynolds et al. 1998).

Molecular hydrogen along our line of sight to 3C 111 associated with the Taurus molecular cloud may explain

the excess. In fact, this gas would not contribute to the 21 cm emission, but the metals/dust associated with it will have opacity in the X-ray band. If about 60% of the gas along the line of sight to 3C 111 is in molecular form rather than atomic, the discrepancy between the 21 cm radio measurements and the X-ray could be resolved.

Pineda et al. (2010) show a linear relationship between CO and extinction A_V in the Taurus molecular cloud. Their results allow to estimate the column of molecular hydrogen H₂ with respect to the extinction: $N_{H_2} = 9.4 \times 10^{20} A_V$. The extinction along the line of sight to 3C 111 is³ 4.53, which gives a molecular column density of $N_{H_2} \simeq 4.3 \times 10^{21}$. This value is indeed consistent with the excess absorption with respect to the atomic H I. This is also consistent with the more general relation between the total column density of H I plus H₂ reported in Bolatto et al. (2013) of $N_H \simeq 1.9 \times 10^{21} A_V \text{ cm}^{-2}$, which provides an estimate of $N_H \sim 8 \times 10^{21} \text{ cm}^{-2}$ toward 3C 111. Finally, this is overall in agreement with the molecular hydrogen column density of $N_{H_2} \simeq 4.5 \times 10^{21} \text{ molecules cm}^{-2}$ estimated from the interstellar CO emission line measurement derived by Bania, Marscher & Barvainis (1991) toward 3C 111. However, we note that the cloud in front of 3C 111 is translucent rather than opaque, and the H₂ to CO ratio is better constrained for opaque clouds.

4. CONCLUSIONS

In this paper we show that the cold absorption detected in the X-ray band toward 3C 111 is indeed of Galactic origin and it is very likely due to a combination of atomic and molecular gas. Therefore, we recommend to use the total Galactic column density here estimated to be $N_H = (7.4 \pm 0.1) \times 10^{21} \text{ cm}^{-2}$ when studying the radio galaxy 3C 111. For instance, a recent spectral energy distribution study of the radio, optical, IR, and X-ray knots in the extended jet of 3C 111 was found to be dependent on the assumed Galactic column (Clauzette et al. 2016). On the other hand, the presence of these complexities toward 3C 111 make this object a very promising background source for multiwavelength studies of the characteristics of the atomic and molecular gas in the Taurus molecular cloud, which is the closest large star-forming region in our Galaxy (e.g., Ungerer et al. 1985; Marscher, Moore & Bania 1993; Moore & Marscher 1995; Güdel et al. 2007). The synergy between future deeper high-energy resolution X-ray observations and multi-wavelength campaigns will allow us to investigate in more details the characteristics of the complex multi-phase medium in the Milky Way, and constrain the composition, elemental abundance, distribution, and

³ From <https://ned.ipac.caltech.edu/>

the presence of dust.

F.T. thanks A. D. Bolatto and A. P. Marscher for the useful comments. F.T. and C.S.R. acknowledges support for this work by the National Aeronautics and Space Administration (NASA) through Chandra Award Number GO4-15103A issued by the Chandra X-ray Observatory Center, which is operated by the Smithsonian Astrophysical Observatory for and on behalf of NASA

under contract NAS8-03060. F.T. acknowledges partial support by the Programma per Giovani Ricercatori - anno 2014 “Rita Levi Montalcini”. E.B. is supported by the European Unions Horizon 2020 research and innovation programme under the Marie SkłodowskaCurie grant agreement no. 655324, and by the ICORE program of the Planning and Budgeting Committee (grant number 1937/12).

REFERENCES

Asplund, M., Grevesse, N., Sauval, A. J., & Scott, P. 2009, *ARA&A*, 47, 481

Ballo, L., Braito, V., Reeves, J. N., Sambruna, R. M., & Tombesi, F. 2011, *MNRAS*, 418, 2367

Bania, T. M., Marscher, A. P., & Barvainis, R. 1991, *AJ*, 101, 2147

Bolatto, A. D., Wolfire, M., & Leroy, A. K. 2013, *ARA&A*, 51, 207

Bordoloi, R., Fox, A. J., Lockman, F. J., et al. 2017, *ApJ*, 834, 191

Braito, V., Reeves, J. N., Sambruna, R. M., & Gofford, J. 2011, *MNRAS*, 414, 2739

Chatterjee, R., Marscher, A. P., Jorstad, S. G., et al. 2011, *ApJ*, 734, 43

Clautice, D., Perlman, E. S., Georganopoulos, M., et al. 2016, *ApJ*, 826, 109

Dickey, J. M., & Lockman, F. J. 1990, *ARA&A*, 28, 215

Dieter, N. H., Welch, W. J., & Romney, J. D. 1976, *ApJL*, 206, L113

Eracleous, M., & Halpern, J. P. 2003, *ApJ*, 599, 886

Fox, A. J., Bordoloi, R., Savage, B. D., et al. 2015, *ApJL*, 799, L7

Gatuzz, E., García, J., Kallman, T. R., Mendoza, C., & Gorczyca, T. W. 2015, *ApJ*, 800, 29

Gofford, J., Reeves, J. N., McLaughlin, D. E., et al. 2015, *MNRAS*, 451, 4169

Grandi, P., Torresi, E., & Stanghellini, C. 2012, *ApJL*, 751, L3

Güdel, M., Briggs, K. R., Arzner, K., et al. 2007, *A&A*, 468, 353

Kalberla, P. M. W., Burton, W. B., Hartmann, D., et al. 2005, *A&A*, 440, 775

Kataoka, J., Stawarz, L., Takahashi, Y., et al. 2011, *ApJ*, 740, 29

Kellermann, K. I., Sramek, R., Schmidt, M., Shaffer, D. B., & Green, R. 1989, *AJ*, 98, 1195

Lewis, K. T., Eracleous, M., Gliozzi, M., Sambruna, R. M., & Mushotzky, R. F. 2005, *ApJ*, 622, 816

Linfield, R., & Perley, R. 1984, *ApJ*, 279, 60

Liszt, H., & Lucas, R. 1996, *A&A*, 314, 917

Liszt, H. S., & Lucas, R. 1998, *A&A*, 339, 561

Lohfink, A. M., Reynolds, C. S., Jorstad, S. G., et al. 2013, *ApJ*, 772, 83

Lohfink, A. M., Ogle, P., Tombesi, F., et al. 2015, *ApJ*, 814, 24

Marscher, A. P., Moore, E. M., & Bania, T. M. 1993, *ApJL*, 419, L101

Moore, E. M., & Marscher, A. P. 1995, *ApJ*, 452, 671

Nicastro, F., Senatore, F., Krongold, Y., Mathur, S., & Elvis, M. 2016, *ApJL*, 828, L12

Ogle, P. M., Davis, S. W., Antonucci, R. R. J., et al. 2005, *ApJ*, 618, 139

Pineda, J. L., Goldsmith, P. F., Chapman, N., et al. 2010, *ApJ*, 721, 686

Reeves, J. N., Sambruna, R. M., Braito, V., & Eracleous, M. 2009, *ApJL*, 702, L187

Reynolds, C. S., Iwasawa, K., Crawford, C. S., & Fabian, A. C. 1998, *MNRAS*, 299, 410

Sambruna, R. M., Eracleous, M., & Mushotzky, R. F. 1999, *ApJ*, 526, 60

Sambruna, R. M., Tombesi, F., Reeves, J. N., et al. 2011, *ApJ*, 734, 105

Schulz, N. S., Cui, W., Canizares, C. R., et al. 2002, *ApJ*, 565, 1141

Tombesi, F., Cappi, M., Reeves, J. N., et al. 2010a, *A&A*, 521, A57

Tombesi, F., Sambruna, R. M., Reeves, J. N., et al. 2010b, *ApJ*, 719, 700

Tombesi, F., Sambruna, R. M., Reeves, J. N., Reynolds, C. S., & Braito, V. 2011, *MNRAS*, 418, L89

Tombesi, F., Sambruna, R. M., Marscher, A. P., et al. 2012, *MNRAS*, 424, 754

Tombesi, F., Reeves, J. N., Reynolds, C. S., García, J., & Lohfink, A. 2013, *MNRAS*, 434, 2707

Tombesi, F., Tazaki, F., Mushotzky, R. F., et al. 2014, *MNRAS*, 443, 2154

Tombesi, F., Reeves, J. N., Kallman, T., et al. 2016, *ApJ*, 830, 98

Tombesi, F., Mushotzky, R. F., Reynolds, C. S., et al. 2017, arXiv:1703.00516

Torresi, E., Grandi, P., Longinotti, A. L., et al. 2010, *MNRAS*, 401, L10

Torresi, E., Grandi, P., Costantini, E., & Palumbo, G. G. C. 2012, *MNRAS*, 419, 321

Ungerechts, H., & Thaddeus, P. 1987, *ApJS*, 63, 645

Ungerer, V., Nguyen-Quang-Rieu, Mauron, N., & Brillet, J. 1985, *A&A*, 146, 123

Urry, C. M., & Padovani, P. 1995, *PASP*, 107, 803

Vermeulen, R. C., & Cohen, M. H. 1994, *ApJ*, 430, 467

Willingale, R., Starling, R. L. C., Beardmore, A. P., Tanvir, N. R., & O’Brien, P. T. 2013, *MNRAS*, 431, 394

Wilms, J., Allen, A., & McCray, R. 2000, *ApJ*, 542, 914